Author's Accepted Manuscript

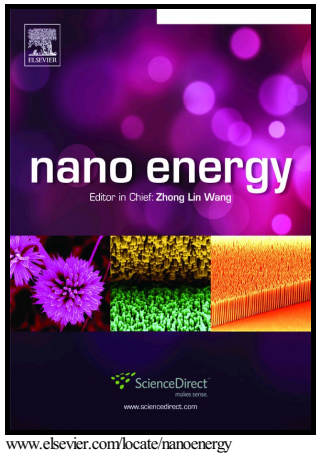

www.elsevier.com/locate/nanoenergy

An effective approach of vapour assisted morphological tailoring for reducing metal defect sites in lead-free, $(CH_3NH_3)_3Bi_2I_9$ Bismuth-based perovskite solar cells for improved performance and long-term stability

Sagar M. Jain, Dibya Phuyal, Matthew L. Davies, Meng Li, Bertrand Philippe, Catherine De Castro, Zhen Qiu, Jinhyun Kim, Trystan Watson, Wing Chung Tsoi, Olof Karis, Håkan Rensmo, Gerrit Boschloo, Tomas Edvinsson, James R. Durrant

PII: S2211-2855(18)30319-7
DOI: https://doi.org/10.1016/j.nanoen.2018.05.003
Reference: NANOEN2711

To appear in: *Nano Energy*

Received date: 5 January 2018
Revised date: 16 April 2018
Accepted date: 1 May 2018

Cite this article as: Sagar M. Jain, Dibya Phuyal, Matthew L. Davies, Meng Li, Bertrand Philippe, Catherine De Castro, Zhen Qiu, Jinhyun Kim, Trystan Watson, Wing Chung Tsoi, Olof Karis, Håkan Rensmo, Gerrit Boschloo, Tomas Edvinsson and James R. Durrant, An effective approach of vapour assisted morphological tailoring for reducing metal defect sites in lead-free, $(CH_3NH_3)_3Bi_2I_9$ Bismuth-based perovskite solar cells for improved performance and long-term stability, *Nano Energy,* https://doi.org/10.1016/j.nanoen.2018.05.003

An effective approach of vapour assisted morphological tailoring for reducing metal defect sites in lead-free, $(CH_3NH_3)_3Bi_2I_9$ Bismuth-based perovskite solar cells for improved performance and long-term stability

Sagar M. Jain[a,b1*], Dibya Phuyal[c1], Matthew L. Davies[a], Meng Li[a,f], Bertrand Philippe[c], Catherine De Castro[a], Zhen Qiu[d], Jinhyun Kim[e], Trystan Watson[a], Wing Chung Tsoi[a], Olof Karis[c], Håkan Rensmo[c], Gerrit Boschloo[b], Tomas Edvinsson[d] and James R. Durrant[a,e]

[a]SPECIFIC, College of Engineering, Swansea University Bay Campus, Fabian Way, SA1 8EN Swansea, United Kingdom.

[b]Department of Chemistry-Ångström Laboratory, Physical Chemistry, Uppsala University, Box 523, SE 751 20 Uppsala, Sweden.

[c]Molecular and Condensed Matter Physics, Department of Physics and Astronomy, Uppsala University, Box 516, SE 751 20 Uppsala, Sweden.

[d]Department of Engineering Sciences, Solid State Physics, Uppsala University, Box 534, SE 751 21 Uppsala, Sweden.

[e]Department of Chemistry and Centre for Plastic Electronics, Imperial College London, Exhibition Road, London SW7 2AZ, United Kingdom.

[f]Institute of Functional Nano and Soft Materials, Soochow University, Suzhou 215000, China.

s.m.jain@swansea.ac.uk
sagarmjain@gmail.com
*Corresponding author. Sagar M. Jain

[1] These authors contributed equally

Abstract

We present a controlled, stepwise formation of methylammonium bismuth iodide $(CH_3NH_3)_3Bi_2I_9$ perovskite films prepared via the vapour assisted solution process (VASP) by exposing BiI_3 films to CH_3NH_3I (MAI) vapours for different reaction times, $(CH_3NH_3)_3Bi_2I_9$ semiconductor films with tunable optoelectronic properties are obtained. Solar cells prepared on mesoporous TiO_2 substrates yielded hysteresis-free efficiencies upto 3.17% with good reproducibility. The good performance is attributed mainly to the homogeneous surface coverage, improved stoichiometry, reduced metallic content in the bulk, and desired optoelectronic properties of the absorbing material. In addition, solar cells prepared using pure BiI_3 films without MAI exposure achieved a power conversion efficiency of 0.34%. The non-encapsulated $(CH_3NH_3)_3Bi_2I_9$ devices were found to be stable for as long as 60 days with only 0.1% drop in efficiency. This controlled formation of $(CH_3NH_3)_3Bi_2I_9$ perovskite films highlights the benefit of the VASP technique to optimize material stoichiometry, morphology, solar cell performance, and long-term durability.

Graphical abstract

We have used vapour assisted solution process technique to prepare lead-free, non-toxic bismuth-based perovskite solar cells using BiI_3 and BiI_3 on reaction with CH_3NH_3I vapours ($MAI_{(v)}$) for different reaction times. By this stoichiometric tailoring and fine-tuning bismuth-based perovskite have shown record breaking performance with 3.17% hysteresis free efficiency (world record so far for $CH_3NH_3BiI_3$ based perovskite solar cells) that retains for more than 60 days (>1440 hours) under continuous 1 sun (Am1.5G) illumination showing a breakthrough in the long-term stability. The figure represents BiI_3 and multicolour absorber layers formed on reaction of BiI_3 with $MAI_{(v)}$ for different reaction time and utilized in making solar devices.

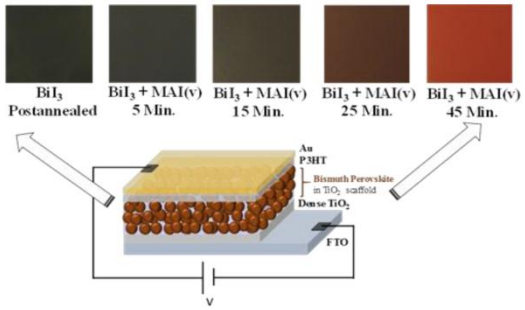

Keywords: Vapour assisted solution process (VASP), Lead free perovskite, $(CH_3NH_3)_3Bi_2I_9$, Morphological tailoring, High resolution x-ray photoelectron (HAXPES) spectroscopy

Introduction

Perovskite solar cells have shown remarkable improvement in power conversion efficiency (PCE) [1] and have reached >22% certified efficiency. Nevertheless, many challenges regarding the stability and toxicity of lead-based perovskite materials remain at the forefront of current research. The toxicity of lead, which is present in a

rather water-soluble form in perovskite solar cells, remains an environmental concern and for this reason there has been several attempts to make lead-free perovskite materials for solar cells. [2 -16] For instance, it has been shown that tin (Sn) based perovskite solar cells can achieve more than 6% efficiency. [16] However, they are generally unstable during the device operation due to the rapid oxidation of Sn^{2+} to Sn^{4+} state. [17 - 18] Antimony and bismuth-based perovskite like materials are increasingly studied as alternatives for toxic lead in perovskite materials due to their optoelectronic properties and stability for photovoltaic applications [13], [19-20]. Furthermore, there are reports of beneficial silver (Ag^{+} ions) doping in bismuth-based perovskite forming bismuth halide double perovskite [5], [21-24]. However, silver iodide is hygroscopic in nature and has poor photostability hindering the stability of these cells. The bismuth based zero-dimensional perovskite shows relatively high band gap (Eg) of 1.8 eV [5], [21 - 24] which makes it a suitable candidate for application in tandem solar cells. Recently, bismuth-triiodide (BiI_3) and $(CH_3NH_3)_3Bi_2I_9$ has been used in solar cells as photoactive materials [25-29] with the highest reported efficiency of 1 % and 1.6% respectively. [28-29] However, there are very few attempts to make pure bismuth triiodide based solar cells and also a lack in systematic investigation on morphological tailoring, a viable route to fully utilize the potential of this material is to fine tune the desired composition and properties for $(CH_3NH_3)_3Bi_2I_9$ material without any doping.

In this direction, we report a vapour assisted solution process (VASP) two-step method to prepare methylammonium bismuth iodide perovskite samples at different

reaction times. Although, VASP method was used for the preparation of lead-based perovskites, [30-31] to date, it has not been exploited to fine-tune the composition of lead-free perovskite materials. In previous work, we studied the formation of $CH_3NH_3PbI_3$ ($MAPbI_3$) by VASP, which proved to be beneficial for the formation of a highly uniform and compact film. [30] Spin coated and annealed BiI_3 films react with methylammonium iodide (MAI) vapours in a similar way as PbI_2 films do [30], [31] resulting in the formation of $(CH_3NH_3)_3Bi_2I_9$ perovskite-like materials. In this process, the primary variable determining the formation of a high-quality film was the reaction time between films of BiI_3 and methylamine as well as hydrogen iodide gas. Reaction time plays a crucial role in yielding a highly crystalline film with low defect concentration. Suppressing the metallic constituents in solution-processed films is beneficial in order to reduce the hole carrier concentration in the films. [32] The VASP process is therefore particularly suitable for light absorbing materials that are sensitive to reduction and synthesis conditions.

We have employed several characterization techniques to probe the optoelectronic properties, surface morphology and chemical constitutes of BiI_3 films and films prepared upon interaction of BiI_3 with MAI vapours for different reaction times.

The record power conversion efficiency of 3.17% was obtained for the solar cells made from BiI_3 + $MAI_{(vapours)}$ with a reaction time of 25 minutes. The champion cells showed high current density of 4.0 mA/cm^2 and an impressive Voc of 1.01 V approaching that of traditional lead-based perovskite solar cells. This work

demonstrates the efficacy of the VASP process in producing highly compact, low metal defects, good quality films and solar cells.

Results and Discussion

The reaction of MAI with BiI_3 was monitored as a function of reaction time using XRD, scanning electron microscopy (SEM), UV-visible spectroscopy, photoluminescence, resonance Raman and X-ray photoelectron spectroscopy.

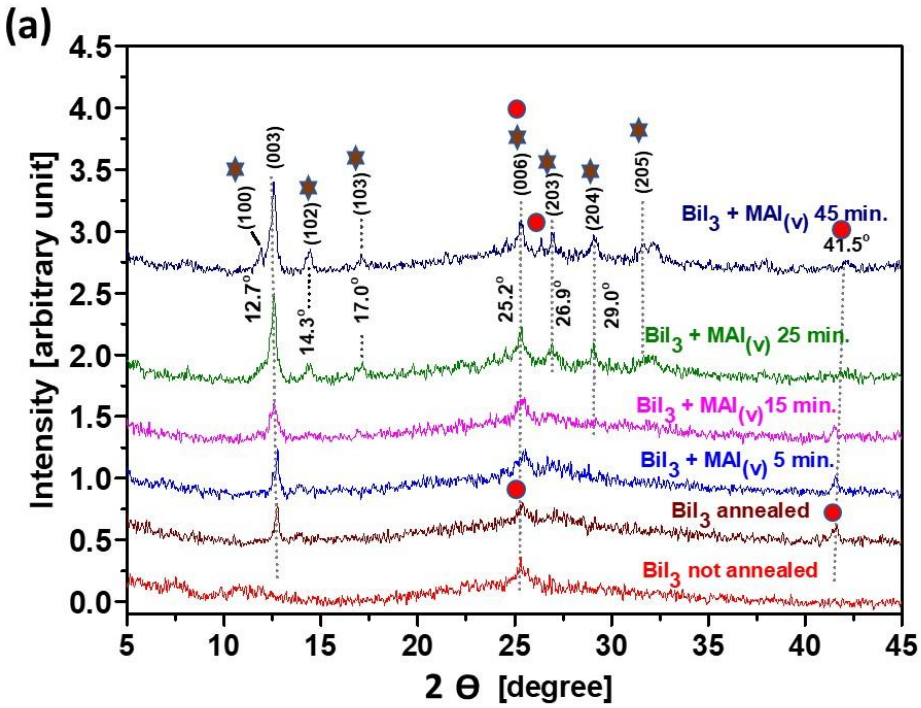

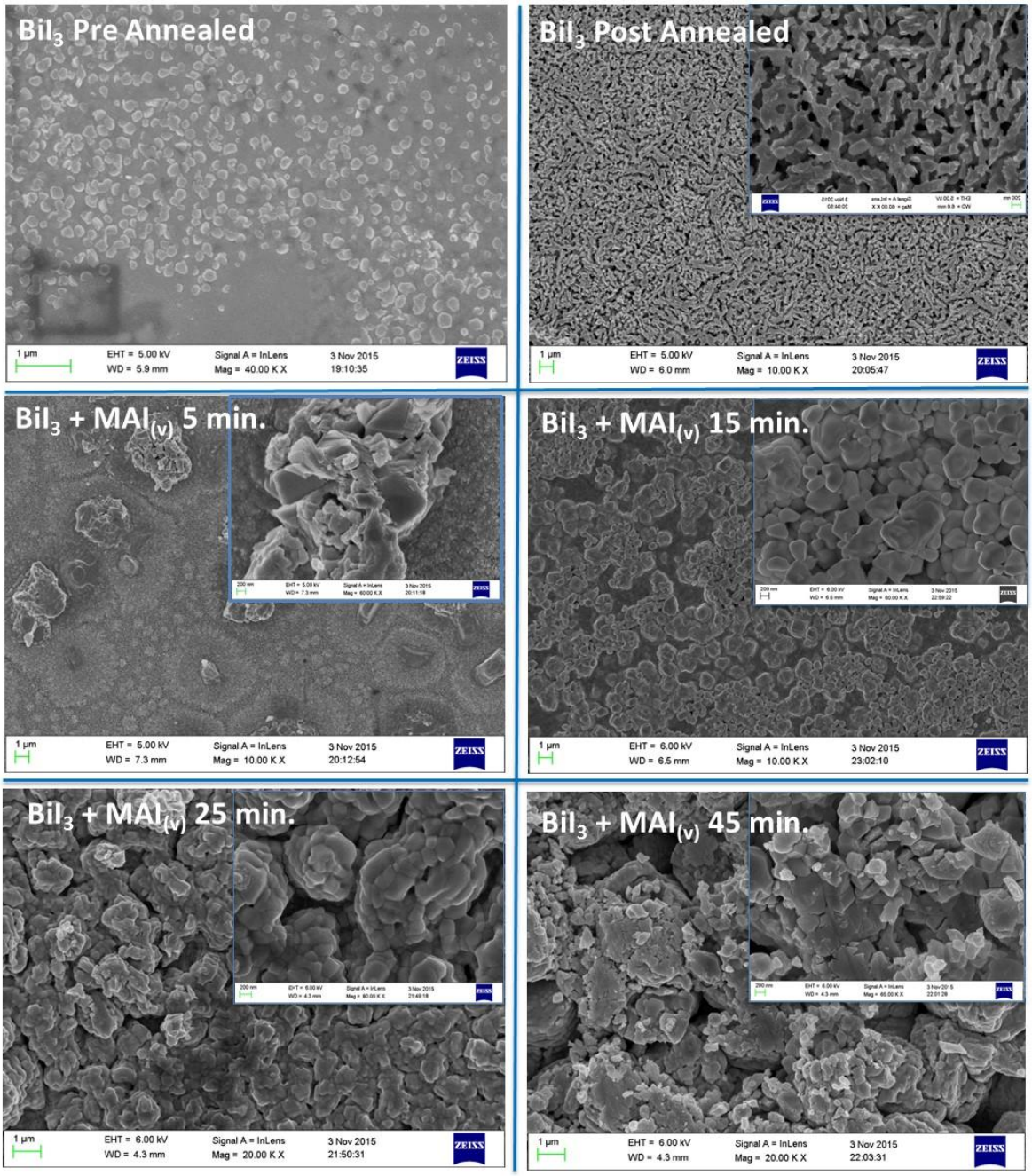

Figure 1. (a) XRD patterns and (b) Top-view SEM images of BiI_3 films before and after annealing and on interaction with MAI vapours for different reaction time. The inserts show magnified views. In the XRD patterns, ★ symbol represents the $(CH_3NH_3)_3Bi_2I_9$ and ● represents the BiI_3 crystalline phase

X-ray diffraction and SEM were used to monitor crystallinity and surface morphology.

Before annealing the spin coated BiI_3 films are mostly amorphous in nature and are

non-uniform with some grains appearing. After annealing at 100^{o}C, these films become more crystalline, evident from XRD (Fig. 1a).

The XRD patterns show a pure hexagonal BiI_3 phase, which is well matched with the reported diffraction data for BiI_3. [15], [33] The increase in intensity of the (003) and (006) orientation from pre-annealed to post annealed samples of BiI_3 films indicates increased crystallization and grain size (Figure 1(a)). On exposure to MAI vapor, which consists of methylamine and hydrogen iodide, there is a colour change from brown/black to red, indicating the conversion to $(CH_3NH_3)_3Bi_2I_9$, this is consistent with the appearance of new peaks in the XRD that can be assigned to $(CH_3NH_3)_3Bi_2I_9$, which is a perovskite-like material. Based on this we propose the following chemical reaction occurring between BiI_3 and MAI. In the first step at high temperatures, solid MAI (CH_3NH_3I) dissociates into CH_3NH_2 and HI gas phase molecules, which subsequently react with BiI_3 to form $(CH_3NH_3)_3Bi_2I_9$.

$$CH_3NH_3I_{(s)} \rightarrow CH_3NH_{2(g)} + HI_{(g)}$$

$$2BiI_{3(s)} + 3CH_3NH_{2(g)} + 3HI_{(g)} \rightarrow (CH_3NH_3)_3Bi_2I_{9\,(s)}$$

Throughout the experiment, we did not observe any peaks that can be assigned to MAI crystals (main reflections at 9^{o}, 19^{o} and 29^{o}. [34-35] This confirms consumption of CH_3NH_3I as a result of perovskite phase formation. Scanning electron microscopy (Figure 1 (b)) shows that spin coated BiI_3 films are inhomogeneous before annealing, after annealing at 100^{O}C for 30 minutes, the deposited BiI_3 crystallizes into a mesoporous film of elongated grains and becomes more homogenous This change is accompanied by an increase in optical absorption (as shown in Figure 3). Annealed

BiI_3 films were selected for making pure BiI_3 based photovoltaic devices and for further reaction with MAI vapours.

The introduction of MAI vapours significantly affected the surface morphology of the films. On increasing reaction time with MAI vapours Figure 1 (b) shows formation of larger sized grains on surface that are continuous throughout the film. Upon longer exposure times, especially the 25 and 45-minutes reaction samples, significantly larger crystal grains formed. This is plausible since the longer exposure to high concentration of MAI vapours at the temperature of 150^{o}C is favourable for the formation of larger crystals [30]. Unlike the previously reported $(CH_3NH_3I)_3Bi_2I_9$ films prepared via one-step solution technique [11] which give inhomogeneous films, our films shows improved homogeneity. This is because the two-step processing involves the formation of BiI_3 grains in first step, which can act as nucleation centres with vapours of CH_3NH_2 and HI, resulting in a more homogeneous surface coverage of $(CH_3NH_3)_3Bi_2I_9$ with rather large grain size as seen from Figure 1(b) SEM surface morphology images. To probe the crystalline as well amorphous bismuth perovskite like phases, we performed resonance Raman spectroscopy on the same samples. The hexagonal phase of BiI_3 belongs to the trigonal crystal system with a hexagonal lattice with space group R-3 (C2 3i in Schoenflies notation) [36] with 4Eg and 4Ag modes are Raman active, and 3Eu and 3Au modes are IR active [37]. The Raman spectra show strong increase in Raman intensity of BiI_3 after annealing in good agreement with the increased crystallinity seen from XRD, Figure 1. The Stokes lines are after annealing seen at 71, 108, 159, 230, and 322 cm^{-1} (Figure 2 a) were the 71

and 108 cm^{-1} lines can be assigned to the Eg and Ag modes, respectively. [34] The slight downshift of the Eg band found here is indicative of large bending type modes in comparison to a pure stretching mode. The band at 159 cm^{-1} has previously been suggested to originate in a second-order Raman band [38], but as the intensity is quite high and that the original band is not enhanced, this assignment is uncertain. The additional high order band seen here (230 cm^{-1}) is consistent with a high crystallinity as seen in XRD and can tentatively be ascribed to combinatorial vibrations (e.g. 71 cm^{-1} + 159 cm^{-1} = 230 cm^{-1}) while the band at 322 cm^{-1} is more uncertain. It can either be from the LO-TO split or as it is quite weak, also a higher order band with three components. The Raman spectra from the reaction with MAI (figure 2b) show a gradual disappearance of the Raman signal in the low wavenumber region and a vibration feature at around 1550 cm^{-1} for intermediate reaction time (15-20 minutes). The loss of Raman activity reveals a successive transformation into a Raman inactive phase, consistent with a transformation to a cubic perovskite phase [39].

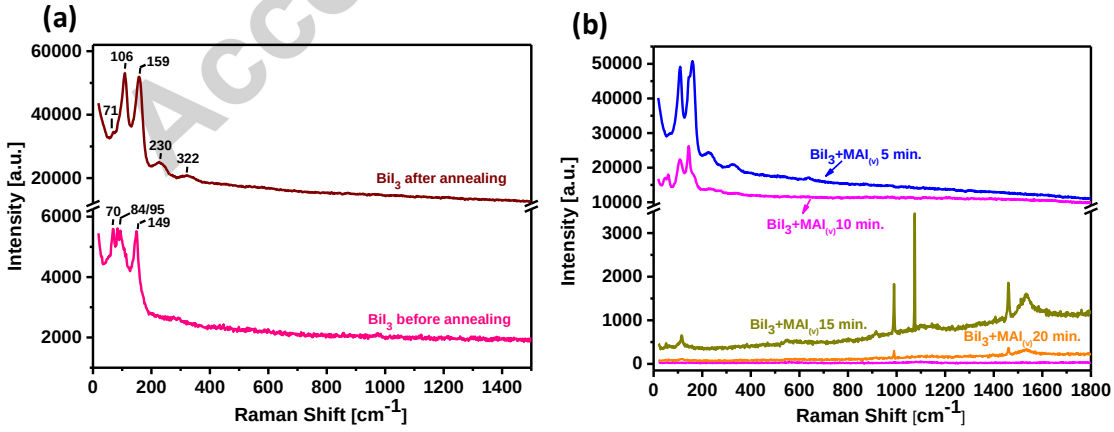

Figure 2. Raman spectra of (a) BiI_3 before and after annealing, and (b) BiI_3 and MAI after different reaction times.

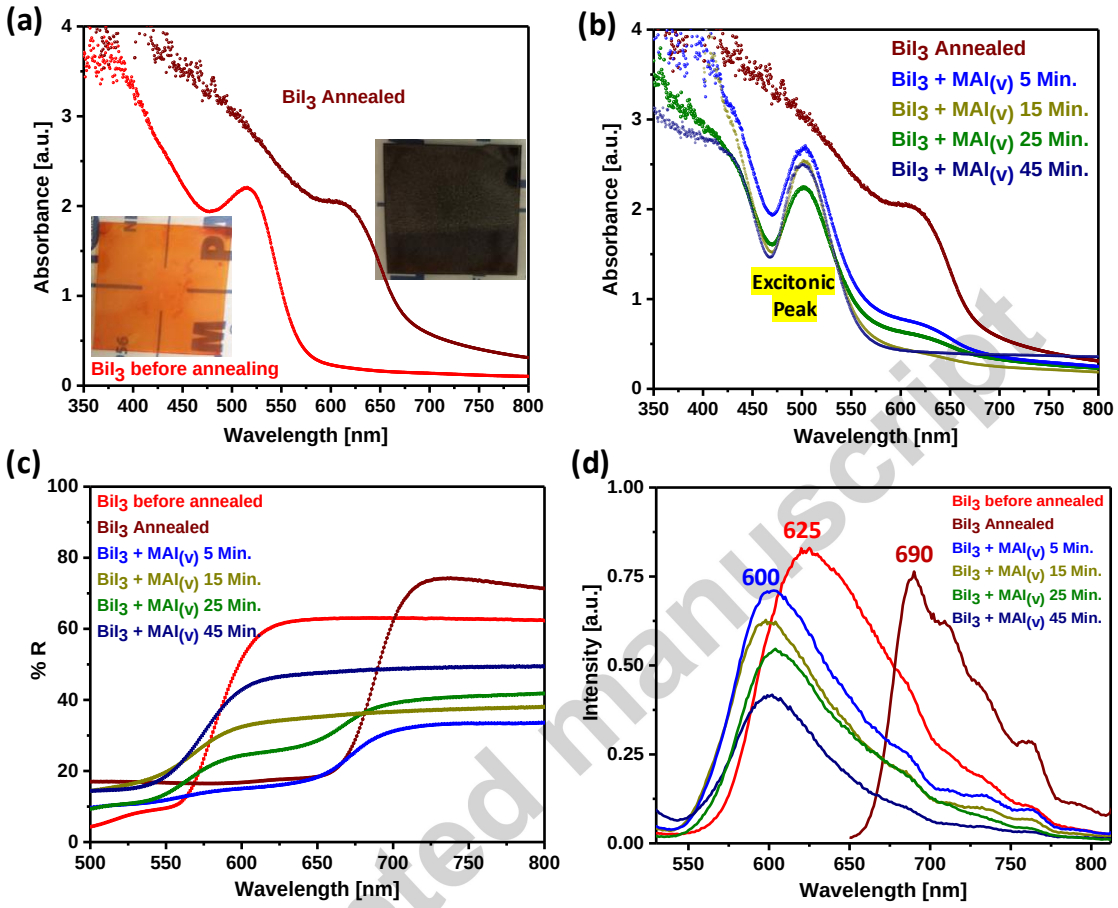

Figure 3. Optical properties of BiI_3 film before and after annealing and on reaction with MAI (CH_3NH_3I) vapours on different reaction time (a) UV-visible spectra of BiI_3 before and after annealing and (b) BiI_3 on interaction with MAI (CH_3NH_3I) vapours on different reaction time. (c) UV-visible reflection measurements, (d) Photoluminescence spectrum.

Ultraviolet-visible (UV-Vis) and photoluminescence (PL) spectra are shown in Figure 3. After annealing the BiI_3 film there is a increased absorption in the visible range and a red-shift of the onset from about 570 to 675 nm (Figure 3(a)), corresponding to a change in respective bandgap from 2.2 eV to 1.8 eV. The bandgap of BiI_3 single

crystals has been reported to be 1.67 eV,[40] similar to the 1.8 eV we observed here. Upon interaction of BiI_3 with MAI vapours for different reaction times, the strong pronounced absorption peak appears around 495 - 516 nm, which is commonly attributed as exciton peak in semiconducting materials (Figure 3 (b)). The peak appears at ~500 nm (maximum intensity) with a shoulder at 625 nm characteristic of two bands involved in the electronic transition. This shoulder at 625 nm decreases with increasing reaction time with MAI vapours. The strong binding energy of the exciton (≈ 400 - 450 meV) may cause poor charge dissociation causing low photocurrent generation. This is a direct result of the interlayer crystal chemistry of $(CH_3NH_3I)_3Bi_2I_9$. The large dielectric mismatch between the large organic cation (MA) and isolated Bi_2I_9 - octahedron is expected to contribute a significant role in excitons dissociation and charge carrier transport. [41] Figure 3 (c) shows the reflectance data measured for the BiI_3 and MAI treated VASP films. The absorption onset of the BiI_3 film was monitored at around 700 nm. The absorption onset of the BiI_3 + MAI vapour films are modified with reaction time [33]. Significantly lower absorption is found for the 5 minutes reaction time films indicating a quick transformation of BiI_3 films to $(CH_3NH_3)_3Bi_2I_9$) composite. As the BiI_3 reaction time with MAI vapours increased the absorption shifted to shorter absorption wavelength range (figure 3(c)). In addition, the formation of $(CH_3NH_3I)_3Bi_2I_9$ composite leads to changes in grains size distribution, causing more light scattering, which can explain the high reflectivity in the near-IR region.

To further delineate the optical properties of the $(CH_3NH_3I)_3Bi_2I_9$ films, photoluminescence (PL) measurements were performed. Figure 3 (d) shows the PL spectra of the BiI_3 films before and after annealing, and with different reaction time with MAI vapours. The measured PL signal for the pre-annealed (spin coated) BiI_3 film is relatively intense broad peak at ≈625 nm (1.98 eV). After annealing the PL is redshifted to a maximum at 690 nm (1.8 eV) with a broad band showing a shoulder at 775 nm. On reaction with MAI vapours at the different reaction times, the films show photoluminescence emission with peaks in the 580-600 nm range as shown in Figure 3(b).

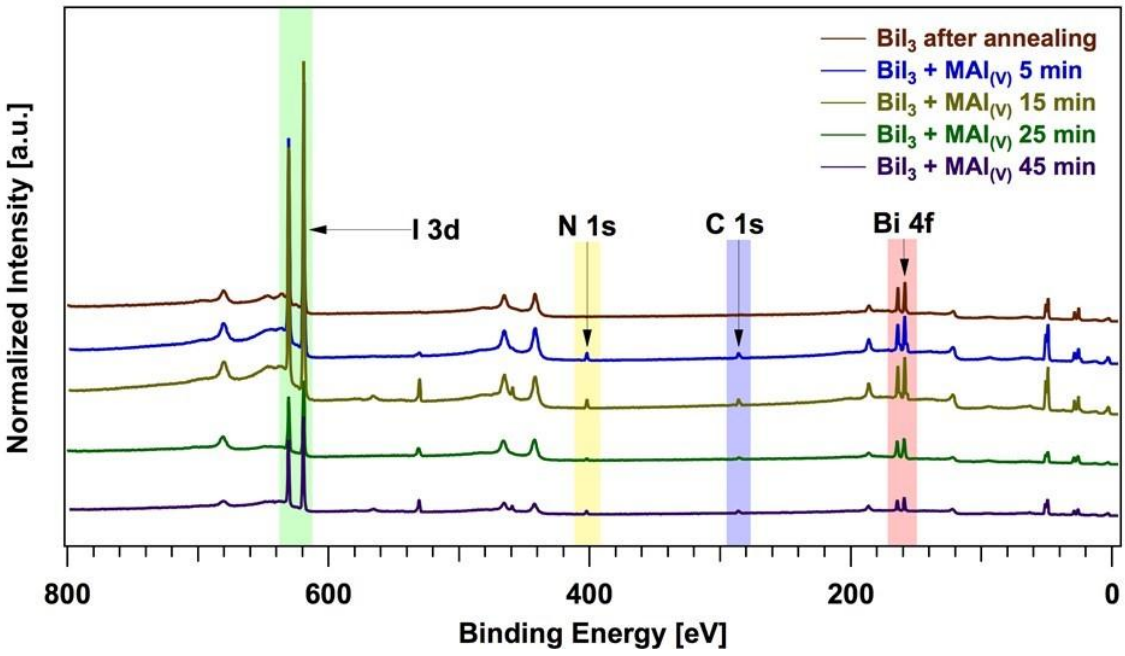

Figure 4. Overview spectra of a precursor material BiI_3 (annealed) and quasi perovskite $(CH_3NH_3I)_3Bi_2I_9$. The spectra are normalized to I 3d5/2 peak, shifted for visualization, and measured with a photon energy of 4000 eV.

Figure 4 shows the photoelectron spectroscopy overview spectra of different $(CH_3NH_3I)_3Bi_2I_9$ films on a TiO_2 substrate along with the annealed BiI_3 film. A photon energy of 4000 eV is used, which is higher than that from traditional in-house Al Kα source (1487 eV) and thus characteristic of a more bulk sensitive characterization of the sample. At 4000 eV, a probing depth (3 × inelastic mean free path) slightly below 20 nm is expected for the core levels reported here. All samples show the distinct core peaks from the deposited materials (i.e. Bi, I, C and N), and no peaks from the substrate (i.e. Ti), which indicates that precursors and the $(CH_3NH_3I)_3Bi_2I_9$ films were deposited thoroughly covering the mesoporous scaffold Titania surface.

The transition from the two precursors to the desired material can be monitored using core level signals. An approximate estimation of the material stoichiometries can be made using the relative intensities of the experimental core levels and taken differential photoionization cross-sections into account. [42] The stoichiometry estimation for I/Bi is listed in Table 1, with values reasonably close to the expected value of 4.5. This stoichiometry points to marginal Iodine deficiencies within the crystal, a common bulk defect found in many organometallic halides [53]

Table 1. HAXPES stoichiometry data for the measured samples.

Sample	BiI_3	$BiI_3 + MAI_{(v)}$ 5 min.	$BiI_3 + MAI_{(v)}$ 15 min.	$BiI_3 + MAI_{(v)}$ 25 min.	$BiI_3 + MAI_{(v)}$ 45 min.
I 4*d*/Bi 5*d*	3.03	4.31	4.30	4.50	4.28
I 3*d*/N 1*s*	-	2.94	2.95	2.82	2.46

The iodine-to-nitrogen ratio is also listed, and the values also commensurate with the expected value of 3. The conversion of BiI_3 and MAI vapours into $(CH_3NH_3)_3Bi_2I_9$ in the VASP process occurs within five minutes with minor variations untill we reach for 45 minutes, where a slight deviation from the desired stoichiometry begins. As discussed later, a reaction time of 45 minute decreases the photovoltaic efficiency as well as the onset for degradation of the material itself. The molar ratios of I : Bi atoms were calculated from the EDX results (Figure S2) for the BiI_3 annealed sample and for BiI_3 + MAI vapours at different reaction time of 5 min., 25 min. and 45 min., being ≈ 3.1, 4.1 and 4.3 respectively. These values are a close match with the HAXPES stoichiometric data obtained in Table 1, and discussed above.

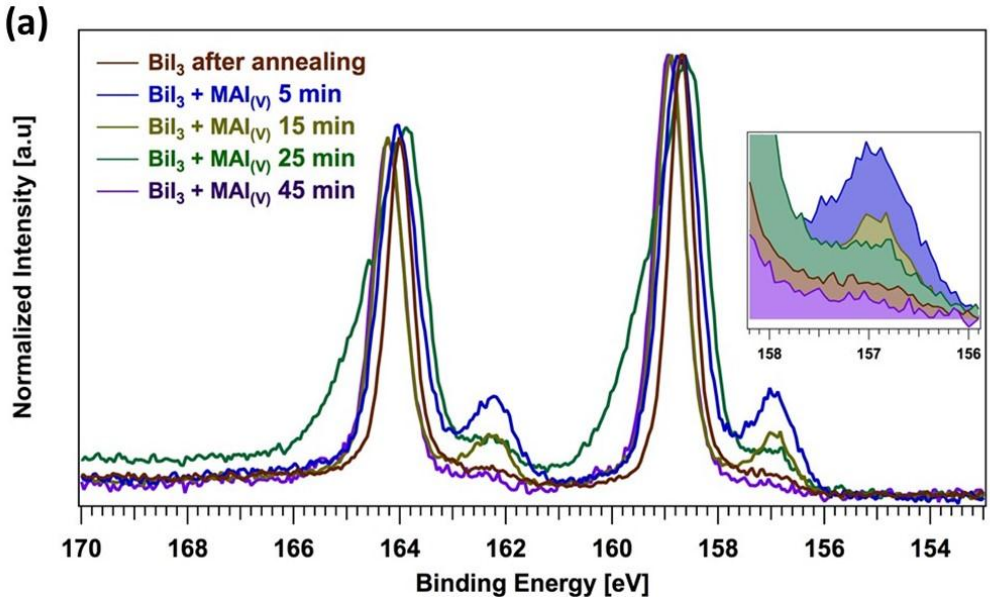

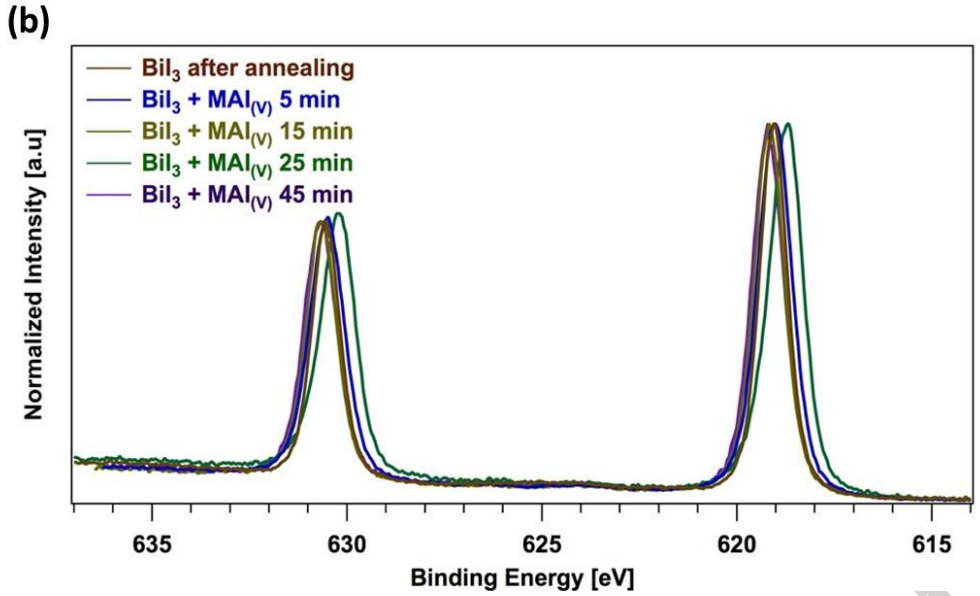

Figure 5 (a) Core-level peak for Bi *4f* and (b) I *3d*. The inset of the Bi *4f signal* shows the metallic portion to the spectra, decreasing with increasing reaction time with MAI, a validation of increased crystallization.

The experimental Bi 4*f* and I 3*d* signals are presented in Figure 5. The main contribution of the main line peak is around 159 eV, indicative of Bi in the Bi^{3+} oxidation state [11]. The Bi 4*f* binding energy positions for the BiI_3 as well the different reaction timed samples are separated by 350 meV. The shoulder peaks at lower binding energy (~157 eV) is metallic Bi^0, which is expected due to the likely decomposition organic metal halides and BiI_3. [43] A discernible trend is observed as we go from sample BiI_3 + $MAI_{(v)}$ 5min. to BiI_3 + $MAI_{(v)}$ 45 minute (an increase of reaction times with MAI, *inset*), is a decrease in the metallic Bi^0 component. This leads to a better control in film quality and a lower possibility of iodine vacancies in the crystal lattice. The improved stoichiometry and overall film quality is seen through sharpening and increased intensity of diffraction peaks (Figure 1(a)). In addition, deconvolution of the Bi 4f spectra indicate that the metallic content

decreases from 20% for 5 minutes to about 2% for 45 minutes, demonstrating the effectiveness of longer vapour exposure times in reducing metallic bismuth in the bulk. In comparison with the conventional one-step or two-step process, the metallic content is still persisting in the material during this synthesis process [44]. The asymmetric spectral shape for the 25 min. samples is likely the result of an additional phase/oxidation state or due to the decomposition of the precursor material present in the sample. This can likely be the result of air exposure or different coordination around the bismuth metal, compensating for the bismuth voids and vacancies in the crystal matrix. Nevertheless, this sample is still follows the trend in decreased metallic content with increased reaction times. This suggests that thicker films reduce metallic bismuth with improved crystallinity. As HAXPES is surface sensitive technique therefore we do not ignore the presence of BiI_3 in the bulk of the composite films formed by BiI_3 + MAI(v). The presence of metallic bismuth is likely to have negative consequences on performance by providing nonradiative decay centres in the bulk. Our present results indicate that this coordination of the bismuth atom is still beneficial to device properties, as discussed in the next sections. We also note that the sample does degrade with exposed radiation with increased concentration of metallic bismuth (Supporting Information, Graph S1), and only spectra without such effects are collected and subsequently averaged. The Iodine 3*d* core level peaks are all around a binding energy of 619.3 eV. The spin−orbit split is 11.5 eV in I 3*d*3/2 level for all samples, indicating the anion iodine in each of the samples are in a very similar electronic environment. The separation in core-level

peaks between I 3*d* and Bi 4*f* for all five samples are approximately 460.20 eV, showing that all samples are in the exact same oxidation states, and aided with composition calculation stated earlier, establishes the same structure and stoichiometry regardless of reaction times.

It is known that bismuth-based compounds experience the same benefit as $MAPbI_3$ through the large relativistic effect of the heavy cation, which act to stabilize the oxidation state [45] and increase the bandwidth of the conduction band by a significant lowering of the CB minimum. [46] The partial Density of state (DOS) plots from previous calculations for similar $Cs_3Bi_2I_9$ show that the excitation across the gap for all phases mainly occur from occupied I *p* states with a small contribution of Bi *s* states into empty Bi *p* + I *p* states. [47]

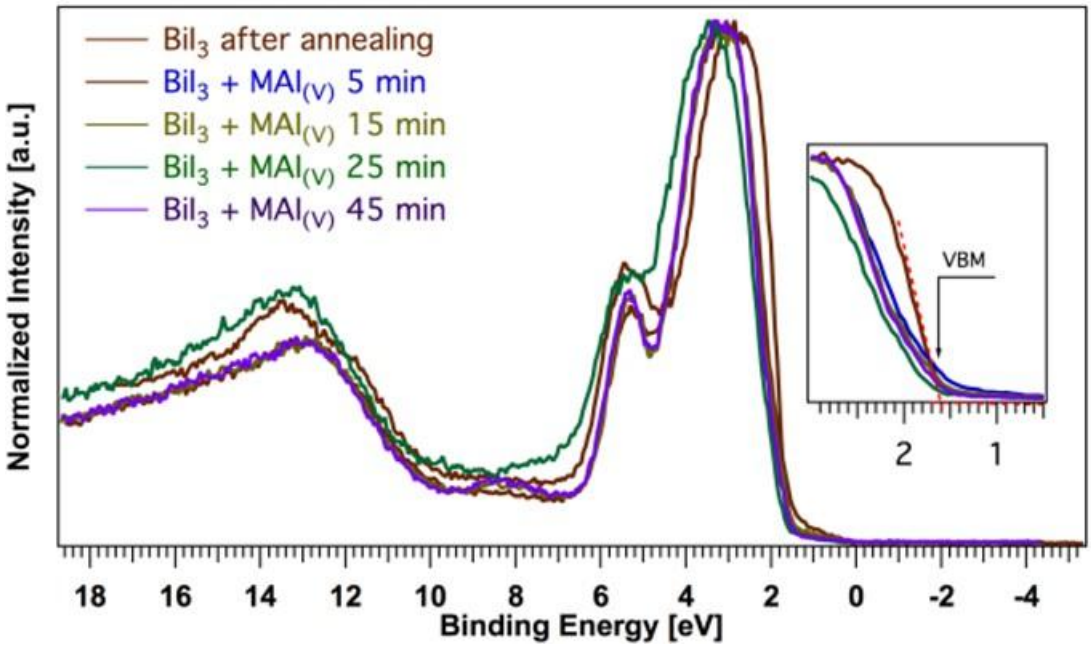

Figure 6. Valence band spectrum for all samples and the annealed BiI_3 film and BiI_3 + $MAI_{(v)}$ for different reaction time. The valence band edge is in same position and the

spectral shape to the precursor, indicating counter cation has limited contribution to the valence states.

We expect that even for a slightly larger cation size such as the methylammonium, the character of the optical transition is expected to be the same. [48] The experimental valence band spectra are shown in Figure 6. The dashed red line (see *inset*) indicates where the linearly extrapolated experimental spectra intersect with the baseline, an estimated measure of the valence band edge position. The VB offset are approximately the same for the entire set, except for reaction time of 5 min., which has a substantially higher metallic bismuth concentration. The extrapolated experimental spectra intersect for nearly all the samples are mostly in line with BiI_3, indicating the corner-sharing counter cation CH_3NH_3 seems not relevant to the density of states in the valence band edge. The main spectral features are the hybridized states around ~3 eV and ~ 5 eV. This region is composed of I 5*p* and Bi 6*p* and lone pair $6s^2$ anti-bonding states. [48] Although the samples were on a nanoporous TiO_2 substrate film, we see very little contribution from the substrate. Generally, the carbon and nitrogen in the organic cation is expected to contribute with some density of states at around 8 and 13 eV, as it for $MAPbI_3$. [44] The lack of such signal comes from a low photoionization cross sections of light elements at high photon energies (*hv* = 4000 eV). The XRD, UV-visible, SEM surface morphology and HEXPES results above show that the introduction of MAI vapours on BiI_3 films significantly improves the crystallization and surface coverage optimizing the quality of the film formed. This stepwise formation of Bismuth-MAI composites effectively

leading to enhanced surface morphology that is usually associated with effective charge transport. To study the effect of these crystalline and morphological properties on the solar cell device performance we have prepared devices with BiI_3 films and BiI_3 films subjected to different reaction times with MAI vapours.

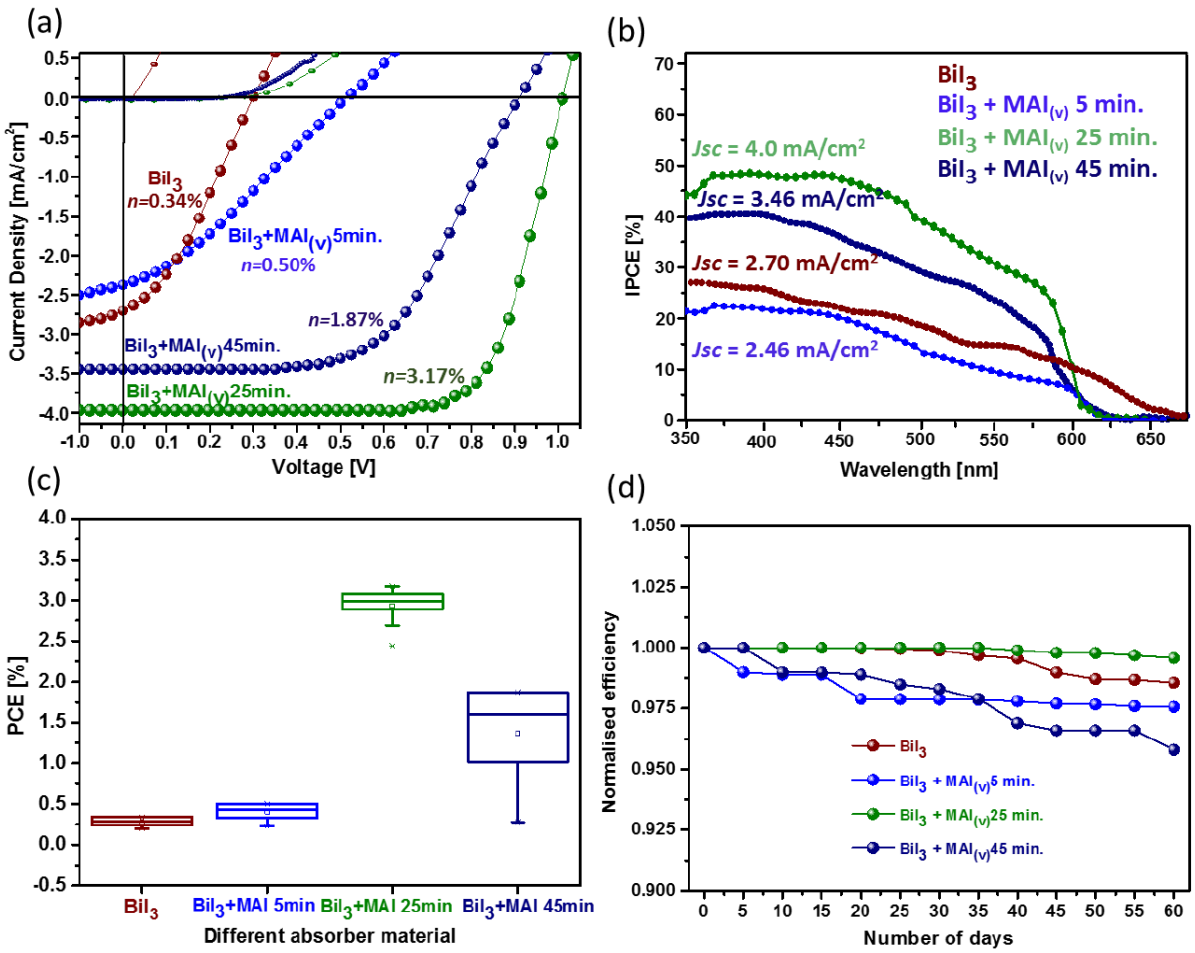

Figure 7. (a) JV characteristics, (b) IPCE, (c) Statistics of PCE of 15 best performing solar cell devices and (d) Stability of non-encapsulated BiI_3 solar cells and devices made from selected BiI_3 + $MAI_{(v)}$ reaction time of 5, 25 and 45 min. respectively

Table 2. Photovoltaic performance at 1000 Wm^{-2} (AM1.5G) of BiI_3 and BiI_3 + $MAI_{(v)}$ (MBI) devices mesoporous devices prepared with different VASP reaction times. All measurements were done at constant scan speed of 10 mVs^{-1}

Devices with different reaction time	Jsc (mA/cm^2)	Voc (V)	FF Fill Factor	Area (cm^{-2})	Efficiency (%)
BiI_3 0 min.	2.71	0.28	0.45	0.126	0.34
BiI_3+$MAI_{(v)}$ 5 min.	2.47	0.47	0.41	0.126	0.50
BiI_3+$MAI_{(v)}$ 25 min.	4.02	1.01	0.78	0.126	3.17
BiI_3+$MAI_{(v)}$ 45 min.	3.48	0.84	0.64	0.126	1.87

Solar cell devices were made using BiI_3 and BiI_3 + $MAI_{(v)}$ films with different reaction time on FTO substrates with a compact TiO_2 and an additional layer of mesoporous TiO_2 prepared by spray pyrolysis and spin coating respectively. P3HT (Poly(3-hexylthiophene-2,5-diyl) is used as the p-type contact for the solar cells. The thickness of the active layer (TiO_2 + perovskite) is 650 - 700 nm (Figure S7). Solar cells prepared using annealed BiI_3 films show a power conversion efficiency of 0.34 % with Jsc = 2.71 mA/cm^2, Voc = 0.28 and *FF* = 0.45. However, this is still low PCE compared to (BiI_3 + MAI) films prepared after different reaction time. The limited efficiency performance of BiI_3 based devices is attributed to the relatively low open circuit voltage of 0.25 V that arises from the mismatch of the valence band maxima of BiI_3 and the hole transport layer (P3HT) used.

Figure 7(a),(b) shows the current-density-voltage (*J-V*) characteristics of an $(CH_3NH_3)_3Bi_2I_9$ solar cell devices measured in illumination using 100 $mWcm^{-2}$ AM 1.5G.

For all solar cells, the short circuit current (Jsc) values obtained from JV characteristics spectrum are well match with the integrated photocurrent density values obtained from IPCE spectrum (Figure S8).

The solar cells prepared by 25 minutes of reaction of BiI_3 with MAI vapours yields record power conversion efficiency of 3.17%, Which is the highest reported PCE to date with a highest current density (Jsc) of 4.02 mA/cm^2, record open circuit voltage (Voc) of 1.01 V and impressive fill factor (FF) of 0.78. All devices shows hysteresis-free behaviour as shown in supporting information Figure S3 and Table S1. At maximum power point tracking for 10 minutes all solar cells show stable power output. (Figure S6) The histogram of photovoltaic performance for best performing 15 solar cell devices for each batch are presented in supporting information, Figure S4. Consistent with the optical absorption of the BiI_3 and BiI_3 + MAI(v) films prepared at different reaction time shows well match with the external quantum efficiency (EQE). The EQE spectrum of devices prepared with BiI_3 shows absorption in visible spectrum around 650 nm, which is close match with optical band gap (1.9 eV) of single crystalline BiI_3 [40]. The open circuit voltage (Voc) shows a steady increase from 0.28 V to 0.91 V upon increasing reaction time from 5 min. to 25 min. The current is rather low 2.47 mA/cm^2 for 5 min. reaction time and is progressively increased for longer exposure times, upto 2.99 mA/cm^2. A low fill factor of 0.41 is observed for BiI_3 + MAI(v) 5 min. reaction time is therefore negatively affects the solar cell performance. With increasing reaction time, the fill factor improves to as high as 0.78 for solar cells prepared with 25 minutes reaction time. The best

performing device with a PCE of 3.17%, is the record reported efficiency for $MABiI_3$ based perovskite materials to date with record open circuit voltage of 1.01 V (FF=0.78), after longer reaction time (45 min.) the short circuit current, Voc and FF is decreased to 3.48 mA cm^{-2} ,0.84 V and 0.64 respectively, limiting the PCE to 1.87%. This decrease in performance at increased reaction time from 25 min. to 45 min. may indicate the degradation of active layer due to the long exposure to high temperature. Table 2 summarizes the photovoltaic performance of the BiI_3 and MBI devices. The trend in PCE was from 0.34 % for BiI_3 and 0.50% 3.17% and 1.8 % for devices prepared with reaction times of 5 min., 25 min. and 45 min. respectively.

This improvement in PCE with reaction time is attributed to the improved homogeneity, which results in improved interface between the HTM and ETM and making charge extraction more efficient and kinetically favourable. Figure S9 (a) - (d) and Table S2 show light intensity dependent Jsc and Voc characteristics of BiI_3 solar cells and solar cells made using BiI_3 and BiI_3 + MAI(v) with reaction times of 5 min., 25 min. and 45 min. All the solar cells show reduction in Jsc and Voc with decreasing light intensity. The champion solar cells made from BiI_3 + MAI(v) with reaction time of 25 min. shows highest Jsc and Voc resulting into the high PCE as compare to the BiI_3 solar cells and solar cells prepared at 5 min. and 45 min. reaction time. One can observe a large difference in the voltage for the dark curve in comparison to voltage under recombination. The precise origin of this is unclear but can be related to the larger halide ion migration expected under illumination and thus passivation of back-

and front contact recombination as well as possible trap state healing in bulk under operation.

Long term stability [49-51] and toxicity [51-52] are critical issues for lead-based perovskite devices. Bismuth is not only a non-toxic element but also possess a better chemical stability in $(CH_3NH_3I)_3Bi_2I_9$ than that of the Pb-based perovskite. The non-encapsulated devices were tested for 60 days. All devices show very small decrease in PCE of 0.1 % after 60 days of time and much improved stability compared to lead-based perovskite. Long-term stability and its evolution in time are shown in Figure 7 (d). In addition, the champion devices were exposed to continuous illumination at 1 sun (AM 1.5G) and simultaneous efficiency measurements for 400 hours (Figure S5) and show negligible drop in efficiency. This improved stability can be attributed to the layered nature of the material as was shown with lead halides perovskites recently. [53] The best performing solar cells (PCE = 3.17%) prepared at 25 min. reaction time shown very good stability with very negligible drop to 3.07% in PCE after 60 days.

Conclusion

We have demonstrated that BiI_3 thin films can be converted into $(CH_3NH_3)_3Bi_2I_9$ perovskite by means of exposure to MAI vapour. The resulting material was used to obtain good performing solar cells. The conversion of BiI_3 mesoporous films to $(CH_3NH_3)_3Bi_2I_9$ perovskite is monitored using the controlled vapor-assisted solution process (VASP) was investigated in detail, using films of BiI_3 and $(CH_3NH_3)_3Bi_2I_9$ on

mesoporous TiO_2. The strong exciton absorption and improved crystallinity and homogeneous surface coverage was monitored by XRD and surface morphology SEM images respectively. The stoichiometric elemental analysis using HAXPES shows formation of $(CH_3NH_3)_3Bi_2I_9$ phase during the entirety of the timed-growth synthesis. Furthermore, HAXPES shows the presence of (metallic) Bi^0. The metal content is substantially reduced after longer vapour-assisted growth (25 and 45 minutes BiI_3 + MAI vapours, mitigating metal defect sites and improving semiconducting properties that resulted in improved photovoltaic efficiency. The variation in the electronic structure in the series is only related to Fermi level of the samples, affecting charge-transfer of photo-excited carriers that are favourable in a mesoporous TiO_2 scaffold. Solar cells made from BiI_3 and $(CH_3NH_3)_3Bi_2I_9$ (different reaction time between precursor BiI_3 + MAI vapours) sample showed improved performance with efficiency of 0.34% for mesoporous Bismuth triiodide and because of improvement in crystallinity and surface morphology on reaction of BiI_3 with MAI vapours record highest efficiencies of 3.17% to 1.87% obtained for devices prepared at relatively long VASP. This phenomenon was mainly attributed to two reasons: (a) Enhanced crystallization and improved surface coverage, which ultimately avoids short circuit, recombination loss caused between perovskite layer and P3HT. (b) Reduction in metal defect sites as observed from high resolution x-ray photoelectron (HAXPES) spectroscopy leads to improved semiconducting behaviour. The findings of this work, specially the reduction of metallic defects as observed from high resolution X-ray photoelectron spectroscopy by using the two-step vapour assisted solution process

methodologies applied is promising to extend the improvement in the performance and stability of other lead free (e.g. antimony and tin) based perovskite solar cells by facile fabrication means.

Acknowledgement

S. M. J. acknowledge Marie Curie COFUND fellowship, Welsh Assembly Government funded Ser-Cymru Solar Project and the Swedish research council (VR) for the financial supports. This project has received funding from the European Union's Horizon 2020 research and innovation programme under the Marie Skłodowska-Curie grant agreement No 663830.

Conflicts of interest

There are no conflicts to declare

AUTHOR INFORMATION

Corresponding Author:

Sagar M. Jain, s.m.jain@swansea.ac.uk ; sagarmjain@gmail.com

Author Contribution

S. M. J. conceived and designed the overall experiments, prepared devices, performed XRD, UV-visible characterization and analysis of the perovskite solar cells, and written the manuscript, D. P. conducted the HAXPES measurements and analysis and participated in writing the manuscript., M.L.D. assisted in analysis of results and edited the manuscript, B. P. assisted the HAXPES measurements, Z. Q. performed Surface morphology (SEM) and EDX measurements, C. D. C. performed photoluminescence measurements, T. W., W. C. T., J. K. and O. K. contributed to the result and analysis, M. L. assisted in stability measurements, T. E. performed resonance Raman measurements and analysis and participated in writing and editing of the manuscript, H. R. guided the HAXPES analysis and measurements, H.R., G.B. T.E. and J. D. edited the manuscript and guided the results and project. All authors contributed to the discussion of the results and commented on the manuscript.

References

(1) https://www.nrel.gov/pv/assets/images/efficiency-chart.png

(2) A. H. Slavney, T. Hu, A. M. Lindenberg and H. I. Karunadasa, J. Am. Chem. Soc.138 (7) (2016) 2138 - 2141

(3) H. H. Li, M. Wang, S. W. Huang, J. B. Liu, X. Lin and Z. R. Chen, *Synthesis and Reactivity in Inorganic, Metal-Organic, and Nano-Metal Chemistry* (41) (2011) 1351-1357

(4) S. Chatterjee, A. Bera and A. J. Pal, ACS Appl. Mater. Interfaces (6) (2014) 20479-20486

(5) A. J. Lehner, D. H. Fabini, H. A. Evans, C. A. Hébert, S. R. Smock, J. Hu, H. Wang, J. W. Zwanziger, M. L. Chabinyc and R. Seshadri, Chem. Mater**.** (27) (2015) 7137- 7148

(6) T. Singh, A. Kulkarni, M. Ikegami and T. Miyasaka, ACS Appl. Mater. Interfaces (8) (2016) 14542-14547

(7) M. Vigneshwaran, T. Ohta, S. Iikubo, G. Kapil, T. S. Ripolles, Y. Ogomi, T. Ma, S. S.Pandey, Q. Shen, T. Toyoda, K. Yoshino, T. Minemoto and S. Hayase, Chem.Mater. 28 (18) (2016) 6436-6440

(8) R. E. Brandt, R. C. Kurchin, R. L. Z. Hoye, J. R. Poindexter, M.W. B. Wilson, S. Sulekar, F. Lenahan, P. X. T. Yen, V. Stevanović, J. C. Nino, M. G. Bawendi and T. Buonassisi, *J.* Phys. Chem. Lett. (6) (2015) 4297-4302

(9) M. Lyu, J.-H. Yun, M. Cai, Y. Jiao, P. V. Bernhardt, M. Zhang, Q. Wang, A. Du, H. Wang, G. Liu and L. Wang, Nano Res**.** 9(3) (2016) 692-702

(10) S. Sun, S. Tominaka, J.-H. Lee, F. Xie, P. D. Bristowe, and A. K. Cheetham, APL Mater. (4) (2016) 031101-1 – 031101-7

(11) B. W. Park, B. Philippe, X. Zhang, H. Rensmo, G. Boschloo and E. M. J. Johansson, Adv. Mater. (2015) (27) 6806-6813

(12) C. M. Tsai, H. P. Wu, S. T. Chang, C. F. Huang, C.H. Wang, S. Narra, Y. W. Yang, C. L. Wang, C. H. Hung and E.W.G. Diau, ACS Energy Lett. (1) (2016) 1086 - 1093

(13) B. Saparov, F. Hong, J. P. Sun, H. S. Duan, W. Meng, S. Cameron, I. G. Hill, Y. Yan, D. B. Mitzi, Chem. Mater. (27) (2015) 5622 - 5632

(14) F. Wei, Z. Deng, S. Sun, F. Xie, G. Kieslich, D. M. Evans, M. A. Carpenter, P. Bristowe, T. Cheetham, Mater. Horiz. (3) (2016) 328-332

(15) C. R. Wang, Q. Yang, K. B. Tang, Y. T. Qian, Chem. Lett. 2 (2) (2001)154

(16) N. K. Noel, S. D. Stranks, A. Abate, C. Wehrenfenning, S. Guarnera, A. A. Haghighirad, A. Sadhanala, G. E. Eperon, S. K. Pathak, M. B. Johnston, A. Petrozza, L. M. Hertz, H. J. Snaith, Energy Environ. Sci. (7) (2014) 3061-3068.

(17) E. S. Parrott, R. L. Milot, T. Stergiopoulos, H. J. Snaith, M. B. Johnston, L. M. Herz, J. Phys. Chem. Lett. (7) (2016) 1321-1326

(18) F. Hao, C. C. Stoumpos, D. H. Cao, R. P. H. Chang, M. G. Kanatzidis, Nat. Photonics (8) (2014) 489-494.

(19) J-C Hebig, I. Kühn, J. Flohre and T. Kirchartz, ACS Energy Lett. 1 (1) (2016) 309-314

(20) M. Vigneshwaram, S. likubo, G. Kapil, T. S. Ripolles, Y. Ogomi, T. Ma, S. S. Pandey, Q. Shen, T. Toyota, K. Yoshino, T. Minemoto and S. Hayase, Chem. Mater. (28) (2016) 6436 - 6440.

(21) Dammak, H.; Yangui, A.; Triki, S.; Abid, Y.; Feki, H., J. Lumin. (161) (2015) 214-220.

(22) N. Kubota, Crys. Res. Technol. (36) (2001) 749-769.

(23) C. Lan, Journal of alloys and compounds (701) (2017) 834-840.

(24) Y. Kim, Z. Yang, A. Jain, O. Voznyy, Gi-H. Kim, M. Liu, L. N. Quan, F. P. G. d. Arquer, R. Comin, J. Z. Fan and E. H. Sargent, Angew. Chem. Int. Ed. (55) (2016) 9586-90.

(25) H. Dammak, A. Yangui, S. Triki, Y. Abid, H. Feki, J. Lumin. (161) (2015) 214-220.

(26) A. J. Lehner, Applied physics letters, (107) (2015) 131109.

(27) S. Öz, J.-C. Hebig, E. Jung, T. Singh, A. Lepcha, S. Olthof, F. Jan, Y. Gao, R. German, P. H. M. van Loosdrecht, K.Meerholz, T. Kirchartz, S. Mathur, Sol. Energ. Mat. Sol. C. (158) (2016) 195-201.

(28) U. H. Hamdeh, R. D. Nelson, B. J. Ryan, U. Bhattacharjee, J. W. Petrich, M. G. Panthani , Chemistry of Materials 28 (18) (2016) 6567-6574.

(29) Z. Zhang, X. Li, X. Xia, Z. Wang, Z. Huang, B. Lei and Y. Gao, J. Phys. Chem. Lett. 8 (17) (2017) 4300–4307

(30) S. M. Jain, B. Philippe, E. M. J. Johnson, B. W. Park, H. Resmo, T. Edvinsson, G. Boschloo, J. Mater. Chem. A **(**4) (2016) 2630 – 2642

(31) Q. Chen, H. Zhou, Z. Hong, S. Luo, H-S Duan, H-H Wang, Y. Liu, G. Li and Y. Yang, J. Am. Chem. Soc. (136) 2 (2014) 622 - 625.

(32) T. Yokoyama, T. B. Song, D. H. Cao, D. H. Cao, C. C. Stoumpos, S. Aramaki and M. G. Kanatzidis, ACS Energy Lett. (2) (2017) 22-28

(33) C. Lan, J. Luo, S. Zhao, C. Zhang, W. Liu, S. Hayase, T. Ma, Journal of Alloys and Compounds (701) (2017) 834-840.

(34) N. J. Jeon, J. H. Noh, Y. C. Kim, W. S. Yang, S. Ryu and S. Il. Seok, Nat. Mater. (13) (2014) 897-903.

(35) S. M. Jain, Z. Qiu, L. Häggman, M. Mirmohades, M. B. Johansson, T. Edvinsson and G. Boschloo, Energy Environ. Sci., (9) (2016) 3770-3782.

(36) J. Trotter and T. Zobel, Z. Kristallogr. (123) (1966) 67-72.

(37) H. C. Hsueh, R. K. Chen, H. Vass, S. J. Clark, G. J. Ackland, W. C-K. Poon, and J. Crain, Physical Review B, (58) (1998) 14812-14822.

(38) Y. Yang, C. Wang, J. Hou, J. Dai, Materials Letters (57) (2003) 2185-2188.

(39) A. Maaej, M. Bahri , Y. Abid , N. Jaidane , Z. B. Lakhdar & A. Lautié, Phase Transitions: A Multinational Journal, 1998, 64:4, 179-190

(40) N. J. Podraza, W. Qiu, B. B. Hinojosa , H. Xu , M. A. Motyka , S. R. Phillpot , J. E. Baciak , S. Trolier-Mckinstry , and J. C. Nino, J. Appl. Phys. (114) (2013) 033110-1 – 033110-8

(41) L. Pedesseau, D. Sapori, B. Traore, R. Robles, H-H. Fang, M. A. Loi, H. Tsai, W. Nie, J-C. Blancon, A. Neukirch, S. Tretiak, A. D. Mohite, C. Katan, J. Even and M. Kepenekian, ACS Nano (10) (2016) 9776-9786.

(42) J. H. Scofield, J. Electron Spectrosc. Relat. Phenom. (8) (1976) 129

(43) B. Brunetti, C. Cavallo, A. Ciccioli, G. Gigli and A. Latini, Scientific Reports (6) (2016) 31896

(44) R. Lindblad, N. K. Jena, B. Philippe, J. Oscarsson, D. Bi, A. Lindblad, S. Mandal, B. Pal, D. D. Sarma, O. Karis, H. Siegbahn, E. M. J. Johansson, M. Odelius, and H. Rensmo. J. Phys. Chem. C 119 (4) 2015 1818 - 1825

(45) J. M. Frost, K. T. Butler, F. Brivio, C. H. Hendon, M. V. Schilfgaarde and A. Walsh, Nano Letters (14) (2014) 2584 - 2590.

(46) A. Walsh, D. J. Payne, R. G. Egdell and G. W. Watson, Chem. Soc. Rev. (40) (2011) 4455-4463.

(47) M. Pazoki, M. B. Johansson, H. Zhu, P. Broqvist, T. Edvinsson, G. Boschloo, and E. M. J. Johansson., J. Phys. Chem. C (120) 2016 29039 - 29046.

(48) X. Huang, S. Huang, P. Biswas and R. Mishra, J. Phys. Chem. C (120) (2016) 28924 - 28932.

(49) G. Niu, X. Guo, L. Wang, *J. Mater. Chem. A*, (3) (2015) 8970-8980

(50) J. Chen, D. Liu, M. J. Al-Marri, L. Nuuttila, H. Lehtivuori, K. Zheng, Sci. China Mater. (59) (2016) 719-727.

(51) L. S. Lujan, N. Espinosa, T. T. L. Olsen, J. Abad, A. Urbina, F. C. Krebs, Adv. Energy Mater. (5) (2015) 1501119.

(52) L. N. Quan, M. Yuan, R. Comin, O. Voznyy, E.M. Beauregard, S. Hoogland, A. Buin, A.R. Kirmani, K. Zhao, A. Amassian, D.H. Kim and A.H. Sargent, J. Am. Chem. Soc. (2016) (138) 2649 -2655

(53) W. Zhang, S. Pathak, N. Sakai, T. Stergiopoulos, P. K. Nayak, N. K. Noel, A. A. Haghighirad, V. M. Burlakov, D. W. deQuilettes, A. Sadhanala, W. Li, L. Wang, D. S. Ginger, R. H. Friend and H. J. Snaith, Nature Comm. (6) (2015):10030

Dr. Sagar M. Jain is a ER Marie Curie COFUND fellow working in SPECIFIC, College of Engineering at Swansea University. Sagar did his Masters in science in Physical chemistry from University of Pune, India. He then carried out his Ph.D. studies in University of Torino, Italy. Before joining Swansea university Sagar was a postdoctoral fellow at Uppsala University, Sweden. Working in solar cell field since last 5 years, Sagar focus on different spectroscopic as well photovoltage characterization techniques to understand structure-property-performance relation in perovskite solar cells (PSCs). One of the several domains of his research involves fundamental investigation to minimize the toxicity of PSCs and using interface engineering approach to improve performance and long-term stability of PSCs. For more information please visit http://www.swansea.ac.uk/staff/engineering/s.m.jain/ E-mail s.m.jain@swansea.ac.uk

Dibya Phuyal is a PhD student at Uppsala University in the Division of Condensed Matter and Molecular Physics. His previous research experience is the development of quantum dot photodetectors as well as dye sensitized solar cells. His current research is on the fabrication of ferroelectric oxide thin films and perovskite halides for optoelectronic devices. A significant component to the research is deriving detailed electronic structures through x-ray spectroscopy techniques such as absorption spectroscopy, photoelectron spectroscopy, and resonant inelastic x-Ray scattering. The spectroscopic data is used to identify material properties and their role in optoelectronic devices.

Dr. Matthew L. Davies is a Senior Lecturer and head of the Applied Photochemistry Group in the Materials Research Centre, College of Engineering at Swansea University. Matthew graduated from the Chemistry Department in Swansea, having completed his MChem, in 2006. He then carried out his PhD studies between Swansea and the University of Coimbra, Portugal, before moving to Bangor University as a post-doctoral researcher. His research focuses on the photochemistry of materials with the aim of improving lifetime, stability, (re-)manufacturability and performance of solar energy device components and correlating this to the scaling of printable photovoltaics. E-mail: m.l.davies@swansea.ac.uk

Meng Li received his B.S. and M. Eng. degree in physics and Materials Science and Engineering at Henan Normal University in 2012 and 2015. He worked as a visiting student in Prof. James Durrant's group at the Swansea University from Apr. 2017 to Oct. 2017. He is currently a Ph.D.

student under the supervision of Prof. Liang-Sheng Liao at Soochow University, China. His current research is focused on device physics of perovskites solar cells and perovskites light emitting diode.

Dr. Bertrand Philippe is currently researcher at Uppsala University at the Division of Molecular and Condensed Matter Physics in the group of Prof. Håkan Rensmo. He completed his PhD in 2013 at Pau University (France) and Uppsala University (Sweden) within a co-shared project and was mainly working on the investigation of novel negative electrode materials for Li-ion batteries via spectroscopic techniques. His current research focuses on the use of photoelectron spectroscopy including in-house and synchrotron based techniques to investigate energy storage and energy conversion materials. Among these systems, he is currently working on perovskite-based materials used for solar cells applications.

Dr. Catherine Suenne De Castro was born in France, then moved to Portugal where she obtained her PhD in Chemistry with specialization in Photochemistry from the University of Coimbra. She is now a Postdoctoral Research Assistant at the Applied Photochemistry Group with the Sustainable Product Engineering Centre for Innovation in Functional Coatings (SPECIFIC). She is based at Swansea University's Material Research Centre within the College of Engineering and supported by the Sêr Solar project. She works mostly on the photophysical characterisation of materials for solar applications and photocatalysis, other research interests include chemosensors, probes and optimization of spectroscopic measurements.

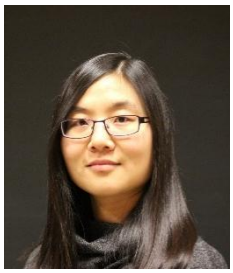

Zhen Qiu received her master degree from the Zhejiang University of Technology, China in 2014. She is now a Ph.D. student in Professor T. Edvinsson's group, Solid State Physics, Uppsala University, Sweden. Her research mainly focuses on the development of low-dimensional transition metal based catalysts and the fundamental understanding in water splitting.

Jinhyun Kim received the B.S. degree in Bio and Nano-chemistry (2009) and the M.S. degree in Nano-chemistry (2012) from Kookmin University, Seoul, Korea, where he was involved with small-molecular organic solar cell using vacuum deposition. Currently, he has been pursuing his PhD. degree at Imperial College London under the supervision of Professor James Durrant. His research is focused on charge carrier dynamics of inorganic–organic hybrid perovskite solar cells by using absorption and emission spectroscopy tools: femto and micro second transient absorption spectroscopy (TAS), and steady-state and transient photoluminescence spectroscopy.

Trystan Watson is an Associate Professor and PV Group Lead at the SPECIFIC Innovation and Knowledge Centre, part of Swansea University, UK. He received his engineering doctorate in materials science from Swansea in 2005 and, following a career in the Steel Industry, returned to academia to pursue research in photovoltaics. His research is mainly focused on the scale-up of thin film printed PV including coating and heating processes compatible with module scale manufacture.

Dr. Wing Chung Tsoi has completed his PhD in organic liquid crystals for solar cells at Hull University and postdoctoral research at University of Sheffield, Imperial College London, and National Physical Laboratory. He has been working as a Senior Research Officer on organic and perovskite photovoltaic (PV) cells at Swansea University in UK. He has published 44 papers in reputed journals and is leading a group on advanced characterization (particularly new/advanced Raman spectroscopy) of organic/perovksite PV materials/devices, stability of organic/perovskite PV materials/devices, and novel/emerging applications of organic/perovskite PV cells, including for indoor application, and power generation windows.

Prof. Olof Karis is since 2011 Professor in Physics at Uppsala University. He is currently the Head of Department of Physics and Astronomy. Prof. Karis received his PhD in Physics at Uppsala University 1997. His field of interest includes developing and implementing X-ray based spectroscopic methodologies and earlier in his carrier he focused on exploring the fundamental aspects of resonant phenomena. In recent years he and his group have investigated electronic structure of functional materials including thin film magnetic materials and specifically focusing on electron dynamics.

Prof. Håkan Rensmo is since 2011 Professor in Physics at the Department of Physics and Astronomy, Uppsala University. He received his PhD in Physical Chemistry at Uppsala University 1998 and did a postdoc in nanochemistry at the Department of Chemistry, University College Dublin. Prof. Rensmo is currently the Head of the Division of Molecular and Condensed Matter Physics. The division develops and implement X-ray based spectroscopic methodologies as powerful tools for the study of atomic processes. His group specifically focuses on fundamental understanding of key processes connected to light to electrical energy conversion and storage.

Gerrit Boschloo received his PhD degree in 1996 at Delft University of Technology, the Netherlands. Currently, he is associate professor at

Uppsala University, Sweden, at the Dept. of Chemistry – Ångström Laboratory, section Physical Chemistry. He leads a research group with main topics dye-sensitized solar cells and perovskite solar cells. The fundamental aspects of these hybrid photovoltaics are investigated using in-house developed in-situ characterization methods. He is author of more than 220 peer-reviewed articles in leading journals.

Prof. Tomas Edvinsson is a professor in Solid State Physics at Uppsala University, Sweden, directing a research group with research within experimental and theoretical photo physics of low dimensional materials, solar cells, and photocatalysis. He is PI and project leader for several national projects from the Swedish research council and the Swedish Energy Agency and part of the Swedish node and work package leader for a European H2020 project coordinated by Helmholtz center, Berlin. He act as reviewer for several national (Swedish, Swiss, German, Netherland research councils) and international grant organizations (ERC, Stanford Global Climate and Energy Project, GCEP).

Prof. James R. Durrant is Professor of Photochemistry in the Department of Chemistry, Imperial College London and Sêr Cymru Solar Professor, University of Swansea. His research addresses the photochemistry of new materials for solar energy conversion – targeting both solar cells (photovoltaics) and solar to fuel (i.e.: artificial photosynthesis). He has published over 400 research papers and was elected a Fellow of the Royal Society in 2017.

Highlights

- For the first time a two-step vapour assisted solution process (VASP) technique was used to systematically react films of BiI_3 with MAI vapours to form perovskite at different reaction time.
- Detailed investigation/characterization for the stepwise formation of $(CH_3NH_3)_3Bi_2I_9$ from the precursors demonstrated a reduction of trap states in the material.
- The effect of metallic content on performance of solar cells as well the formation mechanism of $(CH_3NH_3)_3Bi_2I_9$ was revealed.
- World record hysteresis-free, power conversion efficiency of 3.17% obtained for $(CH_3NH_3)_3Bi_2I_9$ solar cells.
- The devices shown breakthrough in long-term stability, proving stable performance for more than 1,440 hours on continuous 1 sun illumination.